Supplementary Information for Sigloch & Mihalynuk 2013

"Intra-oceanic subduction shaped the assembly of Cordilleran North America"

- **Three supplementary figures (S1, S2, S3)**
- **Discussion of data uncertainties and error propagation**

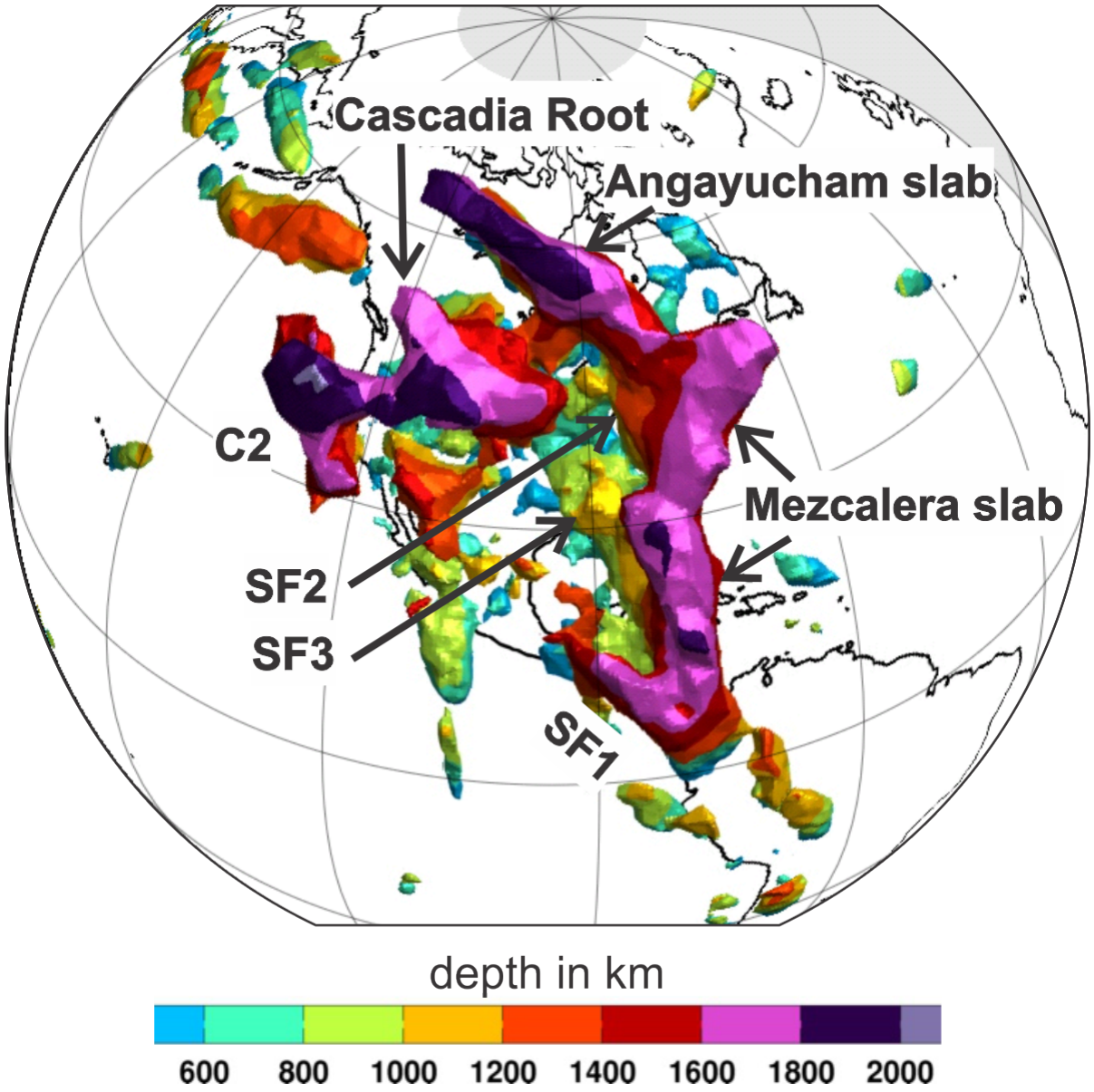
Cascadia Root
Angayucham slab
C2
Mezcalera slab
SF2
SF3
SF1
depth in km
600
800
1000
1200
1400
1600
1800
2000

Figure S1

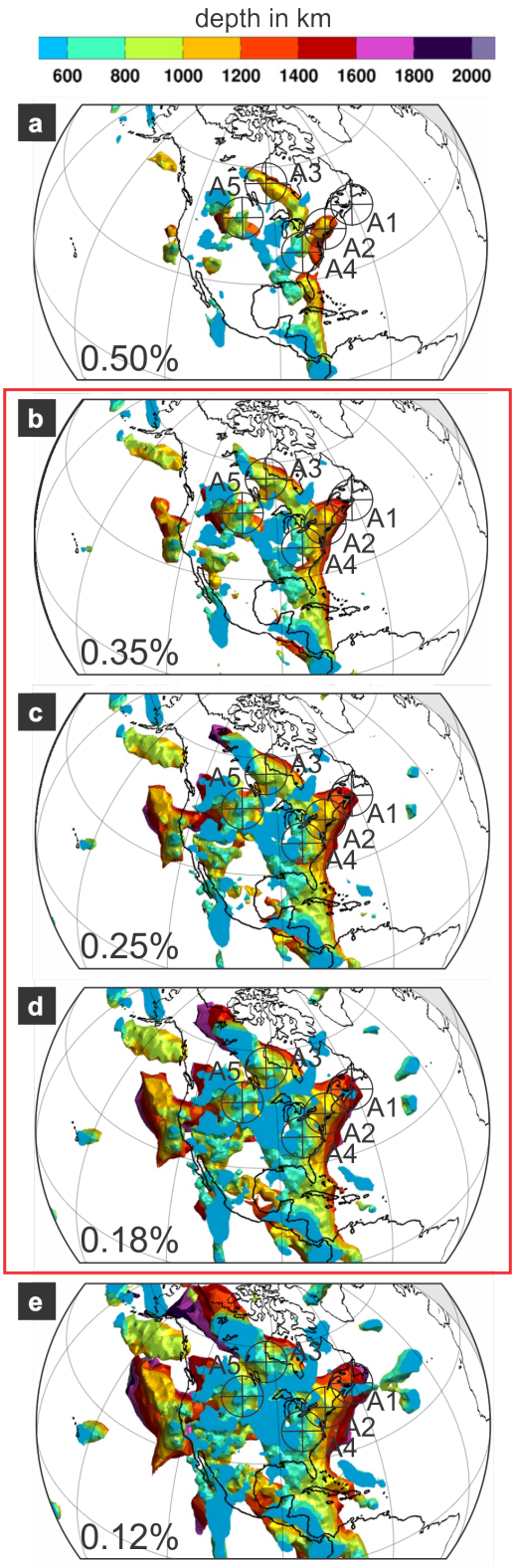
depth in km
600
800
1000
1200
1400
1600
1800
2000
a
A5
A3
A1
A2
A4
0.50%
b
A5
A3
A1
A2
A4
0.35%
c
A5
A3
A1
A2
A4
0.25%
d
A5
A3
A1
A2
A4
0.18%
e
A5
A3
A1
A2
A4
0.12%

Figure S2

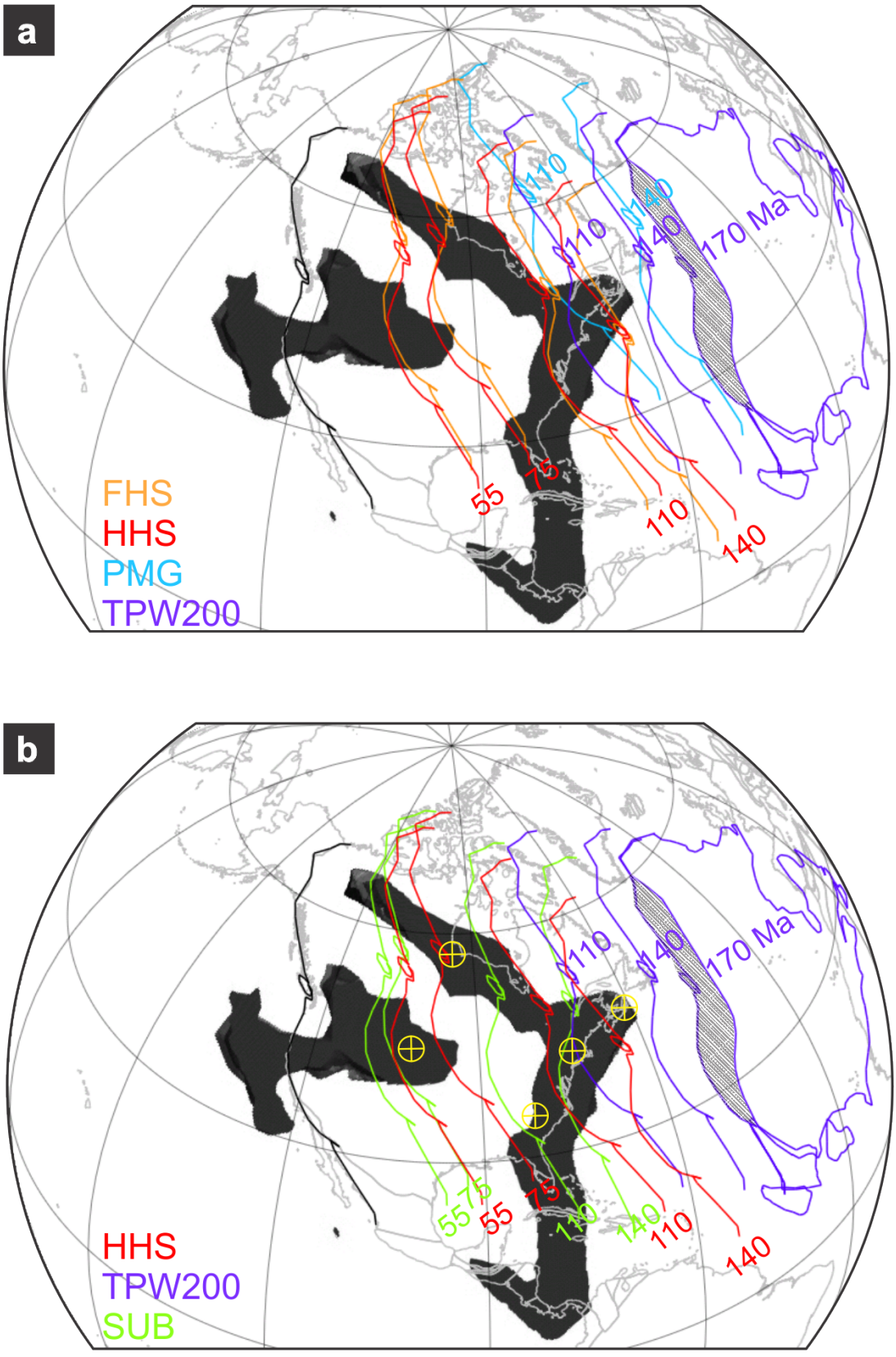
a
FHS
HHS
PMG
TPW200
55
75
110
140
110
140
170 Ma
b
HHS
TPW200
SUB
55
75
110
140
170 Ma

Figure S3

Legends of Supplementary Figures S1-S3

Figure S1. Vertical slab walls ─ inside-out view of seismically fast structure under North America. This 3-D rendering contours fast structure in the P-velocity tomography model by Sigloch 2011 [13], at the same isosurface threshold of dVp/Vp=0.25% as used in figures 1 and 3. It is an "inside-out" view, which moves the deepest structure to the foreground (pink/purple shades at 1800-2000 km), and the shallowest levels to the background (blue, 600-400 km). The perspective corresponds to that of an imaginary observer sitting at the center of the earth, looking upward (except that such a viewpoint would also flip east and west, omitted here). Structure shallower than 400 km is not rendered, since it may represent fast cratonic lithosphere rather than subducted slabs. This view shows most clearly the almost vertical geometry of the deep slab walls below ~800 km depth, the segmentation of the Mezcalera and Angayucham walls, and their clear spatial separation from the crescent-shaped Cascadia Root and slab C2 further west. By contrast, material in the transition zone is smeared out laterally (yellow, green, blue shades). The vertical walls carry the geometric signature of intra-oceanic trenches, which can and do remain stationary over long periods, whereas the shallower slabs were deposited into a trench dragged along by the migrating continent.

Figure S2. Estimation of uncertainties in slab depth. Panels a to e render the same P-wave model [13] at different contouring thresholds dVp/Vp: +0.50%, +0.35%, +0.25%, +0.18%, and +0.12% (the incremental factor is always $\sqrt{2}$). Only fast structure at and below 600 km is shown. The preferred threshold is dVp/Vp=0.25%, used in panel c and in all other figures, and assumed to yield the most probable values for slab depth d. Panels b and d are used to obtain one-sigma error bounds σ_d. The five crosshairs mark calibration points A1-A5. Unit on color bars is depth in km.

Figure S3. Comparison of North America´s westward migration in different absolute reference frames. a: Colored lines show reconstructed western margin over time, in four absolute reference frames. Orange: fixed hotspot FHS [51]; red: hybrid moving hotspot HHS [21]; cyan: paleomagnetic, PMG [50]; purple: true polar wander, TPW/TPW200 [22,52]. Colored labels give time in Ma for their corresponding reference frames; the times used correspond to the four time slices of figure 3. The PMG and TPW frames differ from HHS only prior to 100 Ma, and are shown only at these earlier times. Irregular, dark grey contours are slab outlines at and below 1500 km (identical to those in figure 1a), which should have been subducted by 140 Ma. Present-day landmasses are shown in light grey. The hatched area along the NA margin at 170 Ma represents the assumed uncertainty about true westward extent of the margin (for all times).

b: Same as panel a, except that the subduction reference frame[12], SUB, is compared to HHS and TPW/TPW200. Yellow crosshairs mark calibration points A1-A5. The construction of SUB is fundamentally different from the other frames: it allows for shifts in paleo-longitude if this maximizes the superposition of reconstructed trench lines with imaged slabs. Since the Cretaceous Farallon trench was *assumed* to run along the continental margin, and since it is mapped onto the MEZ/ANG slabs, this frame enforces the Andean-style subduction scenario. This results in a very westerly position of Cretaceous North America that minimizes the extents of the Mezcalera and Angayucham Oceans.

S1. Discussion of data uncertainties and error propagation

We explain the data uncertainties that entered this study, and how they propagate into uncertainty about paleo-margin location, and into the derived slab sinking estimates at points A1-A5. The estimation error has two basic components: uncertainties in plate reconstructions at the surface (when exactly did the western North American margin overlie the calibration points A1 to A5?), and uncertainties about present-day slab geometries (at what depth beneath A1-A5 is the most recently subducted plate relic located today?). Quantitative uncertainty estimates are based only on slab and plate geometries. Timing and spatial estimates from the geological land record do not enter quantitatively, since their role is to validate the kinematically inferred events.

d	current depth (in km) of the upper (youngest) end of the subducted slab wall beneath point Ai, where i=1, 2, 3, 4, 5.
t	time since subduction (in Ma) of this material, i.e., time at which the trench was choked off at the surface because the western NA margin overrode point Ai.
$v = d/t$	slab sinking rate beneath a calibration point Ai (in km/Ma, or mm/a)

Uncertainty in t mainly derives from two sources: uncertainty about the absolute reference frame of the plate reconstruction, and uncertainty about how far west the western NA margin was located over time, compared to stable NA (shaded area in figure 1). We will show that relative timing uncertainties in t are generally larger than relative depth uncertainties.

d and t, the measured values, are assumed to be the most probable values of the associated, Gaussian distributed random variables. Their standard deviations are σ_d and σ_t. Error propagation into σ_v, the uncertainty in sinking rate v, is done according to

$$\sigma_v^2 = v^2 \cdot (\sigma_d^2/d^2 + \sigma_t^2/t^2) \qquad (*)$$

This is the expression for a classical, first-order error propagation[53]: Taylor expansion of v=d/t around point Ai, neglecting terms of order two and higher, assuming that d and t are uncorrelated. We calculate the results for each point Ai separately, again assuming that the five points are uncorrelated. Table S1 summarizes the results. Sections 1.1 and 1.2 explain how the values for d, t, and their uncertainties σ_d and σ_t were obtained. Section 1.3 discusses the sensitivity of the results to assumptions made.

Event Ai (lat/lon)	Description	**$d \pm \sigma_d$ (km)**	**$t \pm \sigma_t$ (Ma)**	**$v \pm \sigma_v$ (mm/a)**	σ_d/d	σ_t/t	σ_v/v
A1 (45.93/-60.67)	Start override MEZ promontory.	**1500 ± 100**	**146 ± 24**	**10 ± 2**	0.07	0.17	0.18
A2 (42.45/-73.12)	End override MEZ promontory.	**1050 ± 50**	**111 ± 8**	**9 ± 1**	0.05	0.07	0.08
A3 (56.74/-94.05)	Override ANG arc.	**850 ± 50**	**74 ± 7**	**12 ± 1**	0.06	0.09	0.11
A4 (33.74/-80.75)	Slab window Farallon, SRC.	**800 ± 50**	**88 ± 3**	**9 ± 1**	0.06	0.03	0.07
A5 (44.72/-103.54)	Override CR arc.	**600 ± 30**	**51 ± 7**	**12 ± 2**	0.05	0.14	0.15

Table S1. Estimates of slab depths d, trench override times t, slab sinking velocities v, and their associated uncertainties σ_d, σ_t, σ_v, at five calibration points A1 to A5.

S1.1 Tomographic uncertainty about present-day slab depth

a) Qualitative uncertainty assessment

The Mezcalera/Angayucham slab walls have been among the most robust features in global-scale body-wave tomography, starting with the work of Grand[9–13,28]. The deep end of the Cascadia Root slab was already visible in some of the earlier studies. Its continuous upward connection to present-day Cascadia subduction was pointed out by Sigloch 2008 [15], hence its identification as a Farallon slab. The model on which we base our discussion here[13] is an inversion of P-wave observations recorded by North American broadband stations, using a cutting-edge waveform inversion technique (multi-frequency tomography) on a global, adaptive grid. Method discussion and formal resolution tests are presented in [13]. The higher resolution compared to global tomography models is largely due to densely spaced stations from the USArray experiment in the western half of the U.S., and waveforms recorded 2005-2008, which were not included in any of the above global models. Our calibration points for sinking rate, especially A3-A5, lie within the mantle subvolume that considerably benefits from resolution improvements afforded by the new USArray data.

b) Quantitative estimates of slab depth

Uncertainty about the depth of the upper (young) end of a subducted slab wall is due to the fact that slab images show diffuse rather than sharp upward truncations. This is expected from tomographic imaging blur, a consequence of incomplete sampling of the subsurface by seismic waves (although in part it may also reflect true geometry of the deformed slab).

Hence the challenge is not to read a depth value off of an isosurface rendering such as figure 1a, but to know which isosurface threshold value best tracks true slab depths. Since true geometries are not knowable, there is no exact way to answer this question. We use the following pragmatic approach for evaluating depth uncertainty: we choose a subjectively preferred isosurface threshold of dVp/Vp=+0.25% (used for Figs 1 and 3, shown again in Fig S2c) and declare this to yield the most probable slab depth readings. The threshold is large enough that obvious imaging artifacts (streaks along wavepaths, diffuse merging of features) are not present, but weak enough that the image as a whole has not started to "erode" significantly.

We also render the model at thresholds stronger by factors of $\sqrt{2}\approx1.4$ (fig. S2b, dVp/Vp=0.35%) and 2.0 (fig. S2a, dVp/Vp=0.50%), and weaker by factors of 1.4 and 2.0 (figs S2d, S2e). The isovalue sequence conveys an intuitive feel for the robustness of model features. End member fig. S2a still contains the cores of all discussed slab walls, but in a severely "eroded" appearance that is physically implausible: slabs should be linearly elongated and interconnected, like their trenches. We can conclude that this rendering threshold is too high. The opposite end member, fig. S2e also shows all salient geometries, but the weak rendering threshold broadens all features, so that the slab walls abut each other and take over most of the mantle volume – not a plausible geometry either.

We assert that the two intermediate thresholds of 0.35% and 0.18% (figs. S2b and S2d) should be robust brackets of the true geometry. They enclose fast anomalies that differ in magnitude by a factor of 2 (quite a large range), but produce images that would not significantly change our conclusions from that of the actual factor used (0.25%, fig. S2c). The first-order observation that supports gradual archipelago override is robust under all thresholds: upward truncations of the slabs walls remain clearly resolved (no westward smearing), and walls located toward the east, i.e., older times, show truncations at greater depths.

As expected, depth value readings beneath A1-A5 are consistently shallower for the weaker rendering threshold, and deeper for the higher threshold. Comparison of figs. S2b and S2d to S2c reveals the variations that we use as standard deviations σ_d in Table S1, second column.

Notes about specific points:

A1 has by far the largest uncertainty, not only due its deeper absolute depth, but also because it is located on a steeply dipping geometry.

At A4, the depths in the two eastern quadrants of the cross hair are used (i.e., slab SF2 before westward step of the trench). The blue material in the two western quadrants is not directly connected to slab SF2 and lies anomalously shallow. It may represent the subducted Shatsky Conjugate plateau itself, and generally appears linked to flat subduction during Laramide times[15].

Event B5, the northwestern truncation of ANG would be an excellent geological calibration point (explosive end of Coast Belt arc volcanism). Its lateral location is probably decently resolved,

but there seems to be significant upward smearing along the wave paths, toward the only surface station in a large circumference in NW Canada.

S1.2 Plate reconstruction uncertainties

a) Qualitative assessment

Figure S3a compares motions of North America in four absolute reference frames, made digitally available by [45]:

- Fixed hotspot frame (FHS) by Müller et al. 1993 [51].
- Hybrid hotspot frame (HHS) by O'Neill et al. 2005 [21], which corrects for differential motion of Indo-Atlantic hotspot tracks from 0-100 Ma. Identical to FHS from 100-140 Ma. This is our preferred reference frame, used to generate figures 1 and 3.
- Hybrid hotspot and paleomagnetic frame (PMG). Identical to HHS from 0-100 Ma, uses a paleomagnetic model from 100-140 Ma by Torsvik et al. [50], where Africa is fixed.
- Hybrid hotspot and TPW-corrected frame (TPW). Identical to HHS from 0-100 Ma, uses a paleomagnetic model corrected for true polar wander between 100-140 Ma, by Steinberger and Torsvik 2008 [52]. Seton et al. 2012 [22] have extended this frame back to 200 Ma (we refer to it as TPW200).

All reference frames agree that two ocean basins should have existed between North America and the Mezcalera/Angayucham slabs at and before 140 Ma. This is the most important assessment of reconstruction uncertainty, since it implies intra-oceanic subduction origins for *all* imaged slab walls, provided they are older than 140 Ma. (That this is indeed the case is shown by the good agreement between predicted and geologically observed collision events, and by the fact that only relatively slow slab sinking at ~10 mm/a is compatible with the observed geometries.)

Conceptually, our reference frame of vertically sinking slab walls is equivalent to hotspot reference frames. As preferred frame, used for figs. 1 and 3, we choose the hybrid hotspot frame (HHS, red in fig. S3). Timing differences compared to the simpler fixed hotspot frame (FHS, orange) will be shown to be marginal, compared to other uncertainties.

Neither hotspot frame can reach back further than 140 Ma, for lack of usable older hotspot tracks. Since the Atlantic spreading record is continuous to ~200 Ma, we can extrapolate that the Angayucham and Mezcalera Oceans prior to 140 Ma would have been at least as wide as at 140 Ma. TPW predicts that already at 140 Ma, the Angayucham and Mezcalera basins were significantly wider than in the hotspot frames, and in TPW200, the basins widen further toward older times (figures 1 and S3). Hence the hotspot frames appear to give conservative (lower) estimates for the extents of these postulated oceans.

Figure S3b shows a fifth absolute reference frame, the subduction reference frame by van der Meer et al. [12], made digitally available by [45]. Despite its conceptual similarity to our vertically sinking slab walls, this reference frame should *not* be used to assess the presence of Angayucham and Mezcalera oceans. By construction, it attempts to minimize the extent of these oceans (by

adding an ad-hoc shift in longitude), because *the Farallon trench is explicitly assumed to run along the NA continental margin*, and reference frame computations attempt to superpose it on the MEZ/ANG slabs at all times. Since the Farallon trench provides some of the strongest constraints on longitude during Cretaceous times, it has strong influence on keeping the Angayucham and Mezcalera oceans as small as possible in this construction. Figure S3b shows that indeed the basins are much narrower in this frame than in all other.

b) Quantitative assessment of plate reconstruction uncertainties

	preferred reference frame			margin uncertainty	alternative reference frame			reconstruction uncertainty	end of subduction	total uncertainty
	τ^{west}	τ^{east}	$\tau = (\tau^{west} + \tau^{east})/2$	$\sigma_\Delta = (\tau^{west} - \tau^{east})/2$	τ_a^{west}	τ_a^{east}	$\tau_a = (\tau_a^{west} + \tau_a^{east})/2$	$\sigma_\tau = \lvert\tau - \tau_a\rvert$	$t = \tau$	$\boldsymbol{\sigma_t}$
A1	~152	140	146	**6**	130	115	123	**24**	**146**	**24**
A2	117	105	111	**6**	110	103	107	**5**	**111**	**8**
A3	80	67	74	**7**	77	66	72	**2**	**74**	**7**
A4	90	85	88	**3**	86	86	86	**2**	**88**	**3**
A5	58	44	51	**7**	59	46	53	**2**	**51**	**7**

Table S2. Reconstruction times and timing uncertainties. The unit of all quantities is Ma, and values are rounded to the nearest integer.

We want to estimate timing uncertainties σ_t for when the NA margin came to overlie points A1-A5, ending subduction there. Two quantities enter the determination of t:

$t = \tau + \Delta$

t is time since subduction (in Ma) of last slab material under Ai, i.e., the time at which the western NA margin actually overrode an intra-oceanic trench at point Ai.

τ is the time at which the plate reconstruction predicts the margin to overlie point Ai. (As the relevant margin line, we could use the present-day coastline, in its relative position to stable North America, but we prefer an imaginary line centered on the hatched area of figure S3, see below.)

Δ is an additional time delay or advance if the true continental margin was not located at the reconstructed position but further inboard or outboard. The hatched area in figure 1 or figure S3

shows the extents to which we consider the margin uncertain. Over time, the margin got both shortened (Sevier, Rocky Mountains, extrusion of escape blocks, terrane transport north), and extended (Cretaceous terrane accretions and Tertiary extension). For the purpose of oceanic trench override, the outboard western terranes would have formed the actual NA margin.

As North America traverses any one calibration point Ai in the GPlates reconstruction software, we record the absolute times when Ai enters and leaves the hatched area. We refer to these times as τ^{west} and τ^{east}, respectively. We assert that the average $(\tau^{west} + \tau^{east})/2$ is the most probable estimate for τ, the time at which the reconstructed margin overlay Ai, meaning the true margin was most likely centered within the hatched area (in terms of traversal time).

The difference $(\tau^{west} - \tau^{east})$ is a measure of timing uncertainty associated with the spatial margin uncertainty. We assert that half this value, $0.5\cdot(\tau^{west} - \tau^{east})$, is a plausible estimate for σ_Δ, the standard deviation of Δ. We consider it equally likely that the true margin lay to the east or to the west of the centered position, i.e., the distribution of Δ has zero mean. Hence the most likely value for t, the absolute time at which we predict end of subduction, is

$t = \tau + 0 = \tau$

Finally we need an estimate for σ_τ, the time uncertainty inherent in plate margin reconstruction τ, which is mainly due to imperfect knowledge of absolute mantle reference frame. For actual values, we compare τ obtained in our preferred reference frame (HHS) to those obtained in an alternative frame (let these be τ_a). The absolute difference $(|\tau - \tau_a|)$ serves as our best guess for σ_τ. As alternative reference frame for assessing points A3-A5, we choose the fixed hotspot frame FHS. For point A1 and A2, we use frame TPW200.

In summary, for each point Ai, we measure the following values in GPlates:

$\tau = (\tau^{west} + \tau^{east})/2$	time of override predicted by plate reconstruction
$\sigma_\tau = \|\tau - \tau_a\|$	reconstruction uncertainty due to absolute reference frame
$\sigma_\Delta = 0.5\cdot(\tau^{west} - \tau^{east})$	additional override uncertainty due to uncertain margin

We propagate these uncertainties into the actually desired quantity $t \pm \sigma_\tau$ (Tables S1, S2), according to:

$$\sigma_t^2 = \sigma_\tau^2 + \sigma_\Delta^2$$

S1.3 Sensitivity to assumptions

Relative reconstruction timing uncertainties σ_t/t usually exceed relative depth uncertainties σ_d/d (Table S1). Both contribute symmetrically to the sinking rate uncertainties in expression (*) above, so that timing errors dominate the overall error, although not dramatically.

In turn, overall timing uncertainty σ_t is due mostly to σ_Δ, i.e., to uncertainty about the westward extent of North America´s paleo-margin. (The exception is the oldest point A1, where reference

frame uncertainty σ_τ dominates.) If we assumed a margin uncertainty twice as large as we did (hatched area roughly twice as wide from west to east), then overall timing uncertainty σ_t would roughly double for A2-A5 (but remain nearly the same for A1), and average sinking rate uncertainty would be σ_v = ±2 mm/a instead of ±1 mm/a.

Hence correct assumptions on the width and shape of the hatched area, which are geologically challenging, have significant influence on overall uncertainty estimates. Shape – rather than just width – is relevant because σ_Δ depends on how obliquely the continent traverses a calibration point A1. Oblique trajectories result in larger uncertainties, e.g., for A5.

We assumed that the intra-oceanic trenches (and hence calibration points) ran centered above the imaged slab outlines. Since those have widened laterally to 400-700 km since sinking to the lower mantle, it is conceivable that the trenches were offset toward one side or the other of the imaged center line. Swaths of spatial uncertainty parallel to this line might have been included, analogous to margin uncertainty, but the standard deviations to assign to them would have been very speculative (100-200 km?).

The uncertainty about absolute reference frame σ_τ is surprisingly small, only 2-5 Ma (except for A1, where it becomes an order of magnitude larger). The small uncertainty at earlier times reflects the difference between fixed and moving hotspots, [51] versus [21]); it might be instructive to compare to alternative reference frames by other workers. However, in order to exceed uncertainties due to paleo-margin extent (typically 6-7 Ma), the uncertainties in absolute reference frame would have to increase by a factor of two or three.

Before 100Ma, absolute reference frames diverge significantly (figure S3) and start to dominate absolute errors. Our alternative frame for point A1 and A2 is TPW/TPW200. It predicts override of A1 at 130 Ma – much later than the preferred frame, at ~152 Ma. (This latter value, τ^{west}(A1) ~ 152 Ma is an approximate value in itself, since the hotspot frame does not reach back beyond 140 Ma. We had to assume that MEZ promontory override from A1 to A2 took the same amount of time for the eastern edge as for the western edge of the hatched area, 35 Ma:

$$\tau^{east}(A1) - \tau^{east}(A2) = 140\ Ma - 105\ Ma = 35\ Ma \quad \rightarrow \tau^{west}(A1) = \tau^{west}(A2) + 35\ Ma = 152\ Ma.$$

Despite large uncertainties, using point A1 for calibration has intuitive appeal. The eastward MEZ promontory predicts onset of deformation in a localized region, today´s Pacific Northwest, rather than simultaneously along the entire margin, which is confirmed by the geological land record of the Foreland Fold and Thrust Belt.

REFERENCES

1. Coney, P. J., Jones, D. L. & Monger, J. W. H. Cordilleran suspect terranes. *Nature (London)* **288**, 329–333 (1980).
2. Engebretson, D. C., Cox, A. & Gordon, R. *Relative motions between oceanic and continental plates in the Pacific Basin*. **206**, (Geological Society of America (GSA), 1985).
3. Atwater, T. Plate tectonic history of the Northeast Pacific and western North America. (Winterer, E. L., Hussong, D. M. & Decker, R. W.) **N**, 21–72 (Geol. Soc. Am., Denver, CO, United States, 1989).

4. Monger, J. W. H., Price, R. A. & Tempelman-Kluit, D. J. Tectonic accretion and the origin of the two major metamorphic and plutonic welts in the Canadian Cordillera. *Geology* **10**, 70–75 (1982).
5. Mihalynuk, M. G., Nelson, J. & Diakow, L. J. Cache Creek Terrane entrapment: Oroclinal paradox within the Canadian Cordillera. *Tectonics* **13**, 575–595 (1994).
6. Dickinson, W. R. & Lawton, T. F. Carboniferous to Cretaceous assembly and fragmentation of Mexico. *Geological Society of America Bulletin* **113**, 1142–1160 (2001).
7. Moores, E. M. Ophiolites, the Sierra Nevada, 'Cordilleria,' and orogeny along the Pacific and Caribbean margins of North and South America. *International Geology Review* **40**, 40–54 (1998).
8. Johnston, S. T. The great Alaskan terrane wreck; reconciliation of paleomagnetic and geological data in the northern Cordillera. *Earth and Planetary Science Letters* **193**, 259–272 (2001).
9. Grand, S. P., Van der Hilst, R. D. & Widiyantoro, S. Global seismic tomography; a snapshot of convection in the Earth. *GSA Today* **7**, 1–7 (1997).
10. Montelli, R., Nolet, G., Masters, G., Dahlen, F. A. & Hung, S.-H. Global P and PP traveltime tomography: rays versus waves. *Geophysical Journal International* **158**, 637–654 (2004).
11. Li, C., Van der Hilst, R. D., Engdahl, E. R. & Burdick, S. A new global model for P wave speed variations in Earth's mantle. *Geochemistry, Geophysics, Geosystems* **9**, 05018 (2008).
12. Van der Meer, D. G., Spakman, W., Van Hinsbergen, D. J. J., Amaru, M. L. & Torsvik, T. H. Towards absolute plate motions constrained by lower-mantle slab remnants. *Nature Geoscience* **3**, 36–40 (2010).
13. Sigloch, K. Mantle provinces under North America from multifrequency P wave tomography. *Geochemistry, Geophysics, Geosystems* **12**, (2011).
14. Pavlis, G. L., Sigloch, K., Burdick, S., Fouch, M. J. & Vernon, F. L. Unraveling the geometry of the Farallon plate: Synthesis of three-dimensional imaging results from USArray. *Tectonophysics* **532**, 82–102 (2012).
15. Sigloch, K., McQuarrie, N. & Nolet, G. Two-stage subduction history under North America inferred from multiple-frequency tomography. *Nature Geoscience* **1**, 458–462 (2008).
16. Sdrolias, M. & Müller, R. D. Controls on back-arc basin formation. *Geochemistry, Geophysics, Geosystems* **7**, 04016 (2006).
17. Goes, S., Capitanio, F. A., Morra, G., Seton, M. & Giardini, D. Signatures of downgoing plate-buoyancy driven subduction in Cenozoic plate motions. *Physics of the Earth and Planetary Interiors* **184**, 1–13 (2011).
18. Ribe, N. M., Stutzmann, E., Ren, Y. & Van der Hilst, R. Buckling instabilities of subducted lithosphere beneath the transition zone. *Earth and Planetary Science Letters* **254**, 173–179 (2007).
19. Gibert, G., Gerbault, M., Hassani, R. & Tric, E. Dependency of slab geometry on absolute velocities and conditions for cyclicity: insights from numerical modelling. *Geophysical Journal International* **189**, 747–760 (2012).
20. Goes, S., Capitanio, F. A. & Morra, G. Evidence of lower-mantle slab penetration phases in plate motions. *Nature (London)* **451**, 981–984 (2008).

21. O'Neill, C., Müller, D. & Steinberger, B. On the uncertainties in hot spot reconstructions and the significance of moving hot spot reference frames. *Geochemistry, Geophysics, Geosystems* **6**, 04003 (2005).
22. Seton, M. *et al.* Global continental and ocean basin reconstructions since 200 Ma. *Earth-Science Reviews* **113**, 212–270 (2012).
23. Boyden, J. A. *et al.*in *Geoinformatics: Cyberinfrastructure for the Solid Earth Sciences* (Cambridge University Press, 2012).
24. Gurnis, M. *et al.* Plate tectonic reconstructions with continuously closing plates. *Computers and Geosciences* **38**, 35–42 (2012).
25. Morgan, W. J. Convection Plumes in the Lower Mantle. *Nature* **230**, 42–43 (1971).
26. Sager, W. W., Handschumacher, D. W., Hilde, T. W. C. & Bracey, D. R. Tectonic evolution of the northern Pacific plate and Pacific-Farallon Izanagi triple junction in the Late Jurassic and Early Cretaceous (M21-M10). *Tectonophysics* **155**, 345–364 (1988).
27. Bunge, H.-P. & Grand, S. P. Mesozoic plate-motion history below the northeast Pacific Ocean from seismic images of the subducted Farallon slab. *Nature* **405**, 337–340 (2000).
28. Ren, Y., Stutzmann, E., Hilst, R. D. van der & Besse, J. Understanding seismic heterogeneities in the lower mantle beneath the Americas from seismic tomography and plate tectonic history. *Journal of Geophysical Research* **112**, 1–15 (2007).
29. Decker, J. *et al.* Geology of Southwestern Alaska. (Plafker, G. & Berg, H. C.) **G-1**, 285–310 (Geological Society of America, Boulder, CO, United States, 1994).
30. Poulton, T. P. *et al.* Kootenay/Nikanassin/Minnes/Deville/ Success Isopach and Lithofacies, in The Geological Atlas of the Western Canada Sedimentary Basin, Chapter 18. (2013).at <www.ags.gov.ab.ca/publications/abstracts/DIG_2008_0252.html>
31. Saha, A., Basu, A. R., Wakabayashi, J. & Wortman, G. L. Geochemical Evidence for a Subducted Infant Arc in Franciscan High-Grade-Metamorphic Tectonic Blocks. *Geological Society of America Bulletin* **117**, 1318–1335 (2005).
32. Dickinson, W. R. Accretionary Mesozoic-Cenozoic expansion of the Cordilleran continental margin in California and adjacent Oregon. *Geosphere* **4**, 329–353 (2008).
33. Ernst, W. G. Accretion of the Franciscan Complex attending Jurassic-Cretaceous geotectonic development of northern and central California. *Bulletin of the Geological Society of America* **123**, 1667–1678 (2011).
34. Leier, A. L. & Gehrels, G. E. Continental-scale detrital zircon provenance signatures in Lower Cretaceous strata, western North America. *Geology* **39**, 399–402 (2011).
35. Johnston, S. T. *et al.* Yellowstone in Yukon: The Late Cretaceous Carmacks Group. *Geology* **24**, 997–1000 (1996).
36. Van de Zedde, D. M. A. & Wortel, M. J. R. Shallow slab detachment as a transient source of heat at midlithospheric depths. *Tectonics* **20**, 868–882 (2001).
37. McDowell, F. W., Roldan-Quintana, J. & Connelly, J. N. Duration of Late Cretaceous-early Tertiary magmatism in east-central Sonora, Mexico. *Geological Society of America Bulletin* **113**, 521–531 (2001).
38. Gonzalez-Leon, C. M. *et al.* Stratigraphy, geochronology, and geochemistry of the Laramide magmatic arc in north-central Sonora, Mexico. *Geosphere* **7**, 1392–1418 (2011).

39. Liu, L. *et al.* The role of oceanic plateau subduction in the Laramide orogeny. *Nature Geoscience* **3**, 353–357 (2010).
40. Livaccari, R. F., Burke, K. & Sengor, A. M. C. Was the Laramide Orogeny related to subduction of an oceanic plateau? *Nature (London)* **289**, 276–278 (1981).
41. Enkin, R. J., Mahoney, J. B., Baker, J., Riesterer, J. & Haskin, M. L. Deciphering shallow paleomagnetic inclinations: 2. Implications from Late Cretaceous strata overlapping the Insular/Intermontane Superterrane boundary in the southern Canadian Cordillera. *Journal of Geophysical Research B: Solid Earth* **108**, EPM 4–1 – 4–19 (2003).
42. Massey, N. Metchosin Igneous Complex, Southern Vancouver Island - Ophiolite Stratigraphy Developed in an Emergent Island Setting. *Geology* **14**, 602–605 (1986).
43. Wells, R. E. Reconsidering the origin and emplacement of Siletzia. *Abstracts with Programs - Geological Society of America* **39**, 19 (2007).
44. Schmandt, B. & Humphreys, E. Seismically imaged relict slab from the 55 Ma Siletzia accretion to the northwest United States. *Geology* **39**, 175–178 (2011).
45. Shephard, G. E. *et al.* Testing absolute plate reference frames and the implications for the generation of geodynamic mantle heterogeneity structure. *Earth and Planetary Science Letters* **317-318**, 204–217 (2012).
46. Liu, L., Spasojević, S. & Gurnis, M. Reconstructing Farallon Plate Subduction Beneath North America Back to the Late Cretaceous. *Science* **322**, 934–938 (2008).
47. Steinberger, B., Torsvik, T. H. & Becker, T. W. Subduction to the lower mantle – a comparison between geodynamic and tomographic models. *Solid Earth Discussions* **4**, 851–887 (2012).
48. Zhong, S. & Gurnis, M. Mantle Convection with Plates and Mobile, Faulted Plate Margins. *Science* **267**, 838–843 (1995).
49. Meer, D. G. van der, Torsvik, T. H., Spakman, W., Hinsbergen, D. J. J. van & Amaru, M. L. Intra-Panthalassa Ocean subduction zones revealed by fossil arcs and mantle structure. *Nature Geoscience* (2012).doi:10.1038/ngeo1401
50. Torsvik, T. H., Müller, R. D., Van der Voo, R., Steinberger, B. & Gaina, C. Global plate motion frames: Toward a unified model. *Reviews of Geophysics* **46**, 3004 (2008).
51. Müller, R. D., Royer, J.-Y. & Lawver, L. A. Revised plate motions relative to the hotspots from combined Atlantic and Indian Ocean hotspot tracks. *Geology* **21**, 275–278 (1993).
52. Steinberger, B. & Torsvik, T. H. Absolute plate motions and true polar wander in the absence of hotspot tracks. *Nature* **452**, 620–623 (2008).
53. Bevington, P. R. *Data reduction and error analysis for the physical sciences*. (McGraw-Hill, 1969).